

UDC 539.3:537.226.86:534.1

**O. Bezverkhyi, V. Karlash, L. Zinchuk  
S. P. Timoshenko Institute of Mechanics,**

*National Academy of Sciences of Ukraine*

## **FORCED VIBRATIONS OF PIEZOCERAMIC CYLINDRICAL SHELLS**

**Summary.** *This paper is devoted to the analysis of the forced vibrations problem for piezoceramic cylindrical shells in the form of short and high rings with radial polarization. Simultaneously a new simple technique for an experimental-computational determination of energy losses components as well as coupling factors is presented. An iterative determination process is illustrated by admittance calculations in resonance–anti-resonance frequency bands for strong modes.*

*It is shown that the admittance, impedance, phase shifts are independent on exciting electric conditions. Sample power, sample voltage and sample current are very sensitive to loading circumstances.*

*When vibrations of the piezoelectric sample are excited by the constant voltage, the instantaneous power in sample increases at resonance frequency in many times in respect to far-resonant frequencies case. And when vibrations of the piezoelectric sample are excited by the constant current, the instantaneous power in sample decreases at resonance frequency in that ratio. The instantaneous power reaches maximum value at resonances for the constant sample voltage and at anti-resonances for the constant sample current. This fact explains why the constant voltage regime is surrounded by significant nonlinearity but in the constant current regime such phenomenon is absent.*

*The stress state of rings was investigated too. Verification of vibration modes was made using the method of piezotransformer transducer. This method enables to determine the distribution of internal stresses for piezoceramic elements from measurements of the surface distribution of charges. For this purpose a number of small electrode-transducers have been divided in an exterior electrode coating of the cylindrical surface. Its potentials and charges are proportional to the sum of principal stresses. It was established that the greater the ratio of height to the middle diameter of the ring, the higher the level of edge mode and the more the distribution of main stresses is different from the cosine function. In a very short rings edge mode is not registered.*

**Key words:** *piezoelectric resonators, energy losses, coupling factors, cylindrical shells*

**О. Безверхий, докт. фіз.-мат. наук; В. Карлаш, докт. техн. наук;  
Л. Зінчук, канд. фіз.-мат. наук**

*Інститут механіки ім. С.П. Тимошенка НАН України*

## **ВИМУШЕНІ КОЛИВАННЯ П'ЄЗОКЕРАМІЧНИХ ЦИЛІНДРИЧНИХ ОБОЛОНОК**

**Резюме.** *Статтю присвячено аналізу проблеми вимушених коливань п'єзокерамічних циліндричних оболонок у вигляді коротких і високих кілець з радіальною поляризацією. Паралельно наведено просту ітераційну експериментально-обчислювальну методику визначення компонентів втрат енергії та коефіцієнтів зв'язку, яку ілюстровано розрахунками адмітансу коротких і високих кілець. Показано, що адмітанс, імпеданс і фазові кути не залежать від умов електричного навантаження, проте миттєва потужність дуже чутлива до режиму. Цей факт пояснює, чому режим заданої сталої напруги супроводжується значною нелінійністю, а в режимі заданого сталого струму такої нелінійності немає.*

*Також досліджено напружений стан кілець. Встановлено, що чим більше відношення висоти до середнього діаметра кільця, тим вищий рівень крайової моди і тим сильніше розподіл головних напружень відрізняється від косинусоїди. В дуже коротких кільцях крайова мода не ресструється.*

**Ключові слова:** *п'єзоелектричні резонатори, втрати енергії, коефіцієнти зв'язку, циліндричні оболонки.*

**Introduction.** Piezoceramic constructional elements are very suitable for purpose of miniaturization. Ultrasonic motors, actuators and transformers are widely integrated in portable electronic devices, such as mobile phone or digital photo. New highly effective piezoceramics are used in multilayer piezotransformers and ultrasonic sonar systems too [1–3].

When the uniform mechanical stress is applied in a non-center symmetric crystal or polarized piezoceramic sample there is a movement of positive and negative ions, creating an electric charge at the surface. This is a direct piezoelectric effect – a conversion of mechanical energy into electrical energy. When electric field is applied to the sample an elastic strain is produced. This is a converse piezoelectric effect – a conversion of an electric energy into mechanical energy. When an alternating electric field is applied mechanical vibrations are induced, which at appropriate frequency cause mechanical resonance with great strains and stresses. This phenomenon is called a piezoelectric resonance [4–7].

Vibrations of the piezoceramic elements are characterized by a large electromechanical coupling of elastic displacements and stresses [4,5,8]. The internal physical processes nature in such bodies drives to the fact that displacements, strains, stresses, powers, admittance and impedance have both real and imaginary parts [9,10]. To calculate any amplitude it is necessary to account energy losses.

Losses in piezoelectrics are considered now to have three components: dielectric, elastic, and piezoelectric [4,5, 9–12]. The elastic (mechanical) losses are explained as internal imperfections, such as internal friction, domain wall motion and lattice defects. The dielectric losses are produced by such imperfections, as conductivity as well as lattice defects too. And at last the piezoelectric losses are coupled with imperfections of energy conversion process [1,10,11]. It is known the analytical solutions of electroelastic vibrations for bodies of simple geometric form such as bars, rods, disks, circular or cylindrical rings etc [4–6, 10–12]. Usually energy losses components in most cases are relatively small in respect to real parts and may be representing in analytical solutions as imaginary parts of complex parameters [4–6].

The analysis of the efficiency of excitation at resonance/anti-resonance frequencies were made by many authors who took into account the mechanical, dielectric and piezoelectric energy losses. It was established that piezoelectric loss tangent causes changes not only in the total energy losses, but also influences the distribution of the thermal losses in the volume.

Heat generation occurs in the sample uniformly under an off-resonance mainly due to the intensive dielectric loss, while heat is generated primarily at the vibration nodal points via the intensive elastic loss under a resonance and originated from the extensive dielectric loss change with electric field and mechanical stress [1–5, 9–12].

The power behavior of piezotransducers is very sensitive to loading conditions and differs for the constant voltage and the constant current. When piezoelectric sample is excited by the constant voltage the instantaneous power in the sample increases at resonance frequency in many times in respect to off-resonant case. And when sample is excited by the constant current the instantaneous power in sample decreases at resonance frequency in that ratio. Thus, the reason of nonlinearity at constant voltage and its absence at constant current, which authors of [2] observed, is high or low level of an instantaneous power.

This paper deals with the analysis of the forced vibrations problem for piezoceramic cylindrical shells in the form of short and high rings. In parallel a new simple technique of an

experimental-computational determination of energy losses components as well as coupling factors is presented [10]. An iterative determination process is illustrated by admittance calculations in resonance–anti-resonance frequency regions for strong mode of high ring. It is shown that admittance, impedance and phase angles are independent from electric loading conditions but the instantaneous power is very sensitive to regime. This fact explains why the constant voltage regime is surrounded by great nonlinearity but in the constant current regime such phenomena is absent.

**Experimental technique.** The material properties of the polarized piezoceramics elements are transversely isotropic. Such bodies are characterized by various elastic, dielectric and piezoelectric parameters which are described by complex values ( $b = b_1 - jb_2 = b_0(1 - jb_m)$ ) to accurately reproduce the energy losses ( $b_2/b_1 = b_m = \tan \xi$ ) [5,6]. The real parts of the complex parameters are determined on the basis of analytical solutions of simple 1-dimensional problem for the free or forced electroelastic vibrations. The imaginary parts are determined usually on maximum/minimum admittances.

The full set of complex modules for TsTStBS-2 ceramics and their temperature dependencies is reported in monograph [4]. K. Uchino and co-authors [3] investigated new ceramics with extremely low losses in wide loading condition interval and observed sharp quality decreasing when the vibration velocity reaches certain level. S. O. Ural et al [2] established that high power behavior of the piezoceramic resonators strongly depends upon loading conditions and is differ for constant current or constant voltage. At present time mechanical (elastic) loss tangent is determined on resonant frequency, dielectric loss tangent is measured at low frequency (1000 Hz) together with shunting capacity measuring and piezoelectric loss tangent is determined at anti-resonant frequency. In all cases knowledge of maximum/minimum admittances are desired with great accuracy.

The resonance and anti-resonance frequencies are determined in analysis as those frequencies, where phase shifts between the sample's voltage and its current are zero [6,9,10]. It is not lightly to reach such effect in practice, and resonance frequency  $f_r$  is identified with the frequency of maximum admittance  $f_m$ , while the anti-resonant frequency  $f_a$  is identified with the frequency of minimum admittance  $f_n$ .

Usually to measure resonance/anti-resonance frequencies and determine of maximum/minimum admittances so called Mason's four-pole is used (fig.1a) [5,6,8]. Input voltage divider  $R_1$ ,  $R_2$  matches generator's output with measuring circuit and decreases ultrasonic generator's signal in  $(R_1 + R_2)/R_2$  times. In parallel to the output resistor  $R_2$  is included the piezoelement  $PE1$  and loading resistors  $R_3$  or  $R_4$ . The voltmeter  $V1$  measures voltage drop  $U_{pe}$  across the piezoelement  $PE1$  and the voltmeter  $V2$  measures voltage drop  $U_R$  across loading resistors, which are commutated by switcher  $S_1$ . Voltage  $U_R$  is proportional to electrical current  $I_{pe}$  in resistor and sample. The ratio of the current  $I_{pe}$  through the piezoelectric element to the voltage drop  $U_{pe}$  is determined as the admittance

$$Y_{pe} = \frac{I_{pe}}{U_{pe}} = \frac{U_R}{RU_{pe}}. \quad (1)$$

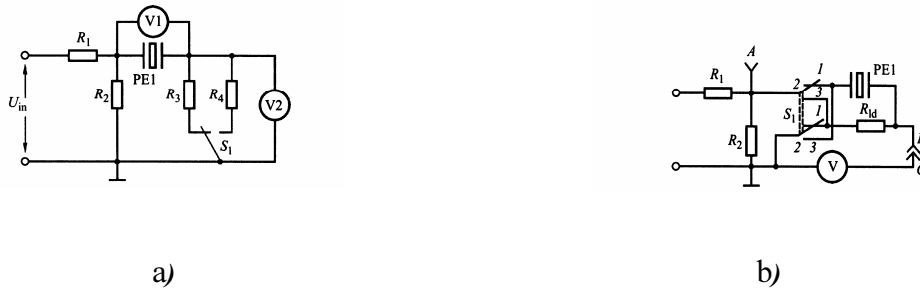


**Figure 1.** Mason-type scheme: a) classic scheme; b) improved scheme [10,11]

**Рисунок 1.** Схеми типу Мезона: а) класична схема; б) удосконалена схема [10,11]

In practice formula (1) not may be used in fig.1a schema, because do not exist such voltmeter, which may be taken for  $V1$  position. For this reason in the schema the voltage  $U_{pe}$  is determined as difference between the input voltage  $U_{in}$  and the voltage  $U_R$ . Instead of exact formula (1) the approximate expression is used

$$Y_{pe1} = \frac{U_R}{R(U_{in} - U_R)}. \quad (2)$$

When the loading resistor and the sample change one another, the next approximate formula may be derived and used

$$Y_{pe2} = \frac{(U_{in} - U_{pe})}{RU_{pe}}. \quad (3)$$

As may be shown all three formulae give identical results on resonance and anti-resonance but results differ strongly a far of these frequencies.

In contrast, the network, which is shown in fig.1b, permits to measure with a great accuracy all voltages  $U_{pe}$ ,  $U_{in}$  and  $U_R$  in a wide range around resonance and anti-resonance by single voltmeter  $V$  and commutation of loading resistor or studying sample [10,11,13,14]. Voltmeter's input (point "C") may be jointed with the voltage divider output (point «A») or common connection of resistor and sample (point «B»). In top switcher position, as shown on fig.1b, this network is analogical to schema on fig.1a and voltmeter measures  $U_R$  voltage. When switcher  $S_1$  is in lower position, voltmeter measures  $U_{pe}$  voltage. This schema realizes three various loading conditions: 1) the constant sample current, 2) the constant sample voltage, 3) the constant input voltage. Based on the experimental data the amplitude-frequency characteristics (AFCh) for different physical parameters of a resonator are plotted on figures below.

The three measured voltages  $U_{pe}$ ,  $U_R$  and  $U_{in}$  create a peculiar characteristic triangle [10–12] and angles between its sides may be calculated with using the cosine theorem (cosine law) as

$$\cos \alpha = \frac{U_{pe}^2 + U_R^2 - U_{in}^2}{2U_{pe}U_R}, \quad \cos \beta = \frac{U_{in}^2 + U_R^2 - U_{pe}^2}{2U_{in}U_R}, \quad \cos \gamma = \frac{U_{in}^2 + U_{pe}^2 - U_R^2}{2U_{in}U_{pe}}. \quad (4)$$

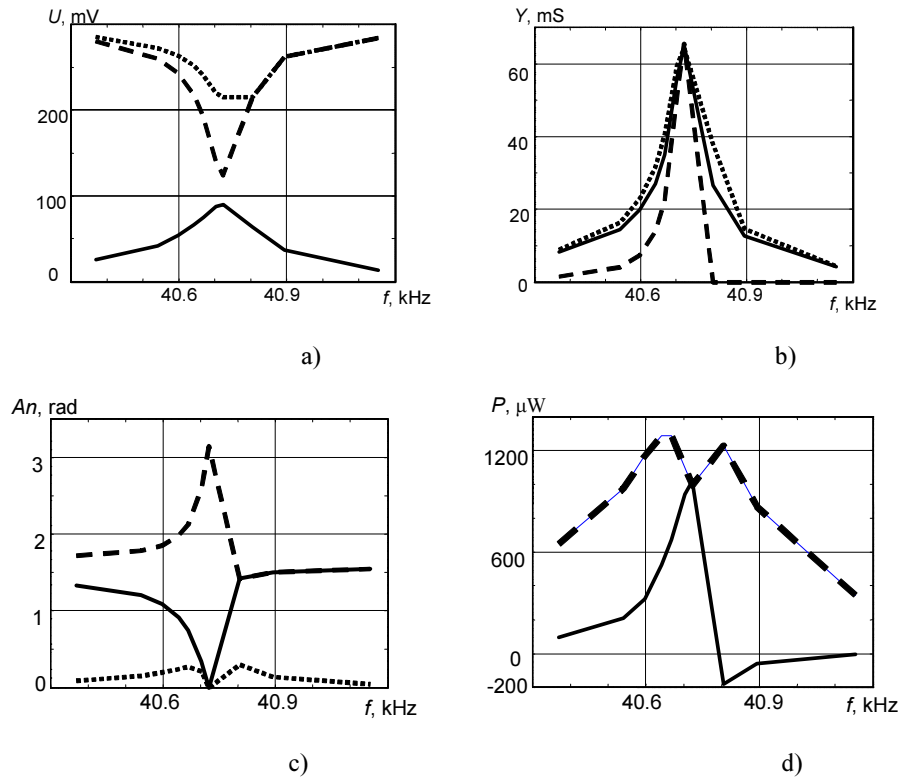


**Figure 2.** Amplitude-frequency characteristics of: a) voltages, b) admittance, c) angles and d) power's components

**Рисунок 2.** Амплітудно-частотні характеристики: а) напруг, б) адмітенсу, в) кутів та д) компонентів потужності

The short ring with dimensions  $27.85 \times 23.08 \times 9.92$  mm made of TBC-3 ceramics had capacity  $C_0 = 6$  nF and the dielectric losses tangent  $\tan \delta = 0.0041$ . fig.2 demonstrates AFCh for voltages  $U_{pe}$ ,  $U_R$  and  $U_{in}$  (in millivolts), the admittance (in millisiemens), angles (in radians) and power's components (in microwatts) respectively at loading resistor 11.2 Ohm. Graphs are obtained for «as is» regime when input voltage  $U_{in} = 285$  mV was chosen on low frequency.

On the graph of fig.2a the voltages  $U_{pe}$ ,  $U_{in}$ ,  $U_R$  are shown as dashed curve, dotted curve and solid line respectively. Next graph (fig.2b) shows the admittance calculated with formulae (1) (solid line), (2) (dotted line) and (3) (dashed line). We can see that at resonance exact expression (1) and approximate expressions (2), (3) gave the same results. The second row of graphs presents triangle angles (fig.2c) and power's components (fig.2d). The angle  $\alpha$  (dotted line) is created by  $U_R$  and  $U_{pe}$  sides. It characterizes a phase shift between the piezoelement current and voltage. The angle  $\beta$  (dashed curve) is created by sides  $U_{in}$  and  $U_R$ . It is according to phase shift between the output generator voltage and the consuming current. At last, the angle  $\gamma$  (solid line) is created by sides  $U_{in}$  and  $U_{pe}$ , i.e., it is the angle between the output voltage of generator and the sample voltage. Phase shifts between the piezoelement

current and voltage rather than between the output generator voltage and the sample voltage at resonance are zero. The phase shift between output generator voltage and the consuming current at resonance reaches  $\pi$ .

The last graph demonstrates instantaneous  $p_1$  (dashed curve) and reactive  $p_2$  (solid curve) powers

$$p_1 = U_{pe} U_R / R, \quad p_2 = p_1 \sin \alpha . \quad (5)$$

The results of measurements are the maximum admittance  $Y_m = 65$  mS at the frequency  $f_m = 40.723$  kHz and the minimum admittance  $Y_n = 0.037$  mS, at the frequency  $f_n = 42.429$  kHz.

The experimental data may be transformed for small signal approximation from the regime “as is” into regimes of constant input voltage, constant sample current, constant sample voltage or the constant sample power with using next formulae

$$U_{in} = U_{in00}, \quad U_{pe} = U_{in00} U_{pe0} / U_{in0}, \quad U_R = U_{in00} U_{R0} / U_{in0};$$

$$U_R = U_{R00}, \quad U_{in} = U_{R00} U_{in0} / U_{R0}, \quad U_{pe} = U_{R00} U_{pe0} / U_{R0};$$

$$U_{pe} = U_{pe00}, \quad U_{in} = U_{pe00} U_{in0} / U_{pe0}, \quad U_R = U_{pe00} U_{R0} / U_{pe0};$$

$$p_0 = p_{00}, \quad t = [p_0 / (U_{R0} U_{pe0})]^{1/2}, \quad U_{pe} = U_{pe0} t, \quad U_R = U_{R0} t, \quad U_{in} = U_{in0} t . \quad (6)$$

Here values  $U_{in0}$ ,  $U_{R0}$ ,  $U_{pe0}$  correspond to the regime “as is” and  $U_{in00}$ ,  $U_{R00}$ ,  $U_{pe00}$ ,  $p_{00}$  are selected arbitrary values that are set well below resonance.

**Iterative technique to determine coupling factor and loss components.** A procedure of coupling factor and loss components determination may be simplified and accuracy may be increased by calculation of the admittance AFCh in frequency range near resonance and anti-resonance. The technique is described below on example of high piezoceramic cylindrical ring vibrations but it may be provided with similar success for somewhat geometry form elements with famous resonant/anti-resonant determinants.

It was shown [10–12] that piezoelectric resonator admittance is the imaginary conductivity of inter-electrode capacity  $C_0$  multiplied on the ratio of the anti-resonance determinant  $\Delta_a(x)$  to the resonance determinant  $\Delta(x)$

$$Y = j\omega C_0 \frac{\Delta_a(x)}{\Delta(x)}, \quad (7)$$

where  $j$  is the imaginary unit,  $\omega$  is the angular frequency, and  $x$  is the running dimensionless frequency, which depend upon geometric sample's form.

The next formulae were derived for the short cylindrical ring and the high cylindrical shell with radial polarization accordingly [12]

$$Y_{sk} = j\omega C_0 \left[ 1 - k_{31}^2 + \frac{k_{31}^2 \omega_r^2}{\omega_r^2 - \omega^2} \right] = j\omega C_0 \frac{\Delta_a(x)}{\Delta(x)},$$

$$\Delta(x) = \omega_r^2 - \omega^2, \Delta_a(x) = (1 - k_{31}^2)\Delta(x) + k_{31}^2 \omega_r^2; \quad (8)$$

$$Y_{hk} = j\omega C_0 \left[ 1 - k_p^2 + \frac{(1 + \nu)k_p^2 \omega_r^2}{2(\omega_r^2 - \omega^2)} \right] = j\omega C_0 \frac{\Delta_a(x)}{\Delta(x)}, \quad (9)$$

$$\Delta(x) = \omega_r^2 - \omega^2, \Delta_a(x) = (1 - k_p^2)\Delta(x) + (1 + \nu)k_p^2 \omega_r^2 / 2.$$

Here  $j$  is the imaginary unit,  $\omega$  and  $\omega_r$  are the angular frequency and the resonant angular frequency,  $k_{31}$  and  $k_p$  are the transverse coupling coefficient and the planar coupling coefficient, and  $\nu$  is Poisson's ratio. The remaining notations coincide with notations in [5, 10–12].

The piezoelectric parameters  $s_{11}$ ,  $\varepsilon_{33}$  and  $d_{31}$  which will be used below we present in the complex form

$$s_{11} = s_{110}(1 - js_{11m}), \varepsilon_{33} = \varepsilon_{330}(1 - j\varepsilon_{33m}), d_{31} = d_{310}(1 - jd_{31m}),$$

where  $s_{11m}$ ,  $\varepsilon_{33m}$  and  $d_{31m}$  are the mechanical, dielectric and piezoelectric loss tangent respectively [6,10].

In a «short» cylindrical ring case the dimensionless frequency is  $x = \omega/\omega_r$  and the real part  $k_{310}$  of the transverse coupling coefficient  $k_{31}$  is determined from the relation

$$k_{310}^2 = \frac{\omega_a^2 - \omega_r^2}{\omega_a^2}, \quad (10)$$

which is known as Mason's formula [1,4,6]. Here  $\omega_r$  and  $\omega_a$  are the resonant angular frequency and the anti-resonant angular frequency.

The maximum admittance  $Y_m$  and the maximum mechanical quality  $Q_m$  are

$$Y_m = \frac{\omega_m C_0 k_{310}^2}{s_{11m}}, Q_m = \frac{Y_m}{\omega_m C_0 k_{310}^2}. \quad (11)$$

In a «high» cylindrical ring case the dimensionless frequency is also  $x = \omega/\omega_r$  and the planar coupling coefficient  $k_p$  is determined from the relation

$$\frac{2(1 - k_p^2)}{(1 + \nu)k_p^2} = \frac{f_m^2}{f_n^2 - f_m^2}. \quad (12)$$

For ease of the admittance calculation we present  $\omega C_0$  in such form

$$\omega C_0 = \frac{2\pi f_0 C_0 x}{x_0} = ax \left( a = \frac{2\pi f_0 C_0}{x_0} \right), \quad (13)$$

where  $f_0$  is the resonant frequency,  $x_0$  and  $x$  are the dimensionless resonant frequency and the running dimensionless frequency respectively.

The iterative experimental-computational procedure of the coupling factor and loss components determination is to compare computer-calculated data with experimental results.

The voltages  $U_{pe}$ ,  $U_R$  and  $U_{in}$  are measured in a wide frequency range around resonance and anti-resonance for the strong mode of high ring and the admittance is determined with formula (1). The amplitude-frequency dependence of admittance is plotted and the frequency of maximum admittance  $f_m$  and the frequency of minimum admittance  $f_n$  are determined.

After that the admittance AFCh in resonance vicinity is calculated with formula (9) and plotted. Wherein the static capacity  $C_0$  and the dielectric loss tangent  $\varepsilon_{33m}$  are measured with alternative current bridge and the value for Poisson's ratio  $\nu$  was taken from experimental data for applicable solid discs [5,6]. In the first iteration step values  $k_p^2$  and  $s_{11m}$  are chosen at random from a predetermined range of existence, and it is assumed that the piezoelectric loss tangent  $d_{31m} \approx \varepsilon_{33m}$ . These parameters are used for further numerical calculations.

According to the graph, the dimensionless frequency of maximum admittance  $x_m$  and the dimensionless frequency of minimum admittance  $x_n$  are determined. The ratio of  $x_n$  to  $x_m$  is compared with measured  $f_n/f_m$  and  $k_p^2$  is corrected. The admittance AFCh in resonance vicinity is calculated with formula (9) and plotted again. If  $x_n/x_m$  is close to  $f_n/f_m$  we will be adjust  $s_{11m}$  to the maximum value of the measured admittance coincided with the corresponding calculated value. When the calculated value for  $Y_m$  approaches the measured value we may go to the anti-resonant region and refine the value of piezoelectric loss tangent  $d_{31m}$ . We select the value for  $d_{31m}$  at which the calculated minimum value of the admittance is close to the measured minimum value of the admittance. Authors' experience shows that acceptable results are obtaining with three or four iterative steps.

Fig.3 shows an example. Here the admittance modulus is plotted as dashed line, the real part of the admittance is plotted as solid line and the imaginary part of the admittance is plotted as dotted line. The right graphics refine the interval near the minimum admittance.

first iteration step (fig.3a) was performed with next data (cylindrical shell with dimensions  $18.5 \times 15.7 \times 22$  mm made of TsTS-19 ceramics):  $C_0 = 14480$  pF,  $\varepsilon_{33m} = 0.0104$ ,  $a = 7.02$  mS,  $\nu = 0.35$ ,  $k_p^2 = 0.2$ ,  $s_{11m} = 0.009$ ,  $d_{31m} = 0.012$ . Measured data were:  $Y_m = 170$  mS,  $Y_n = 0.14$  mS,  $f_m = 77.789$  kHz,  $f_n = 90.039$  kHz,  $f_n/f_m = 1.1574$ . The calculated results  $x_m = 1.0$ ,  $Y_m = 106$  mS,  $x_n = 1.081$ ,  $Y_n = 0.4$  mS,  $x_n/x_m = 1.081$  are not in agreement with the experimental data. It is necessary to increase  $k_p^2$  value.

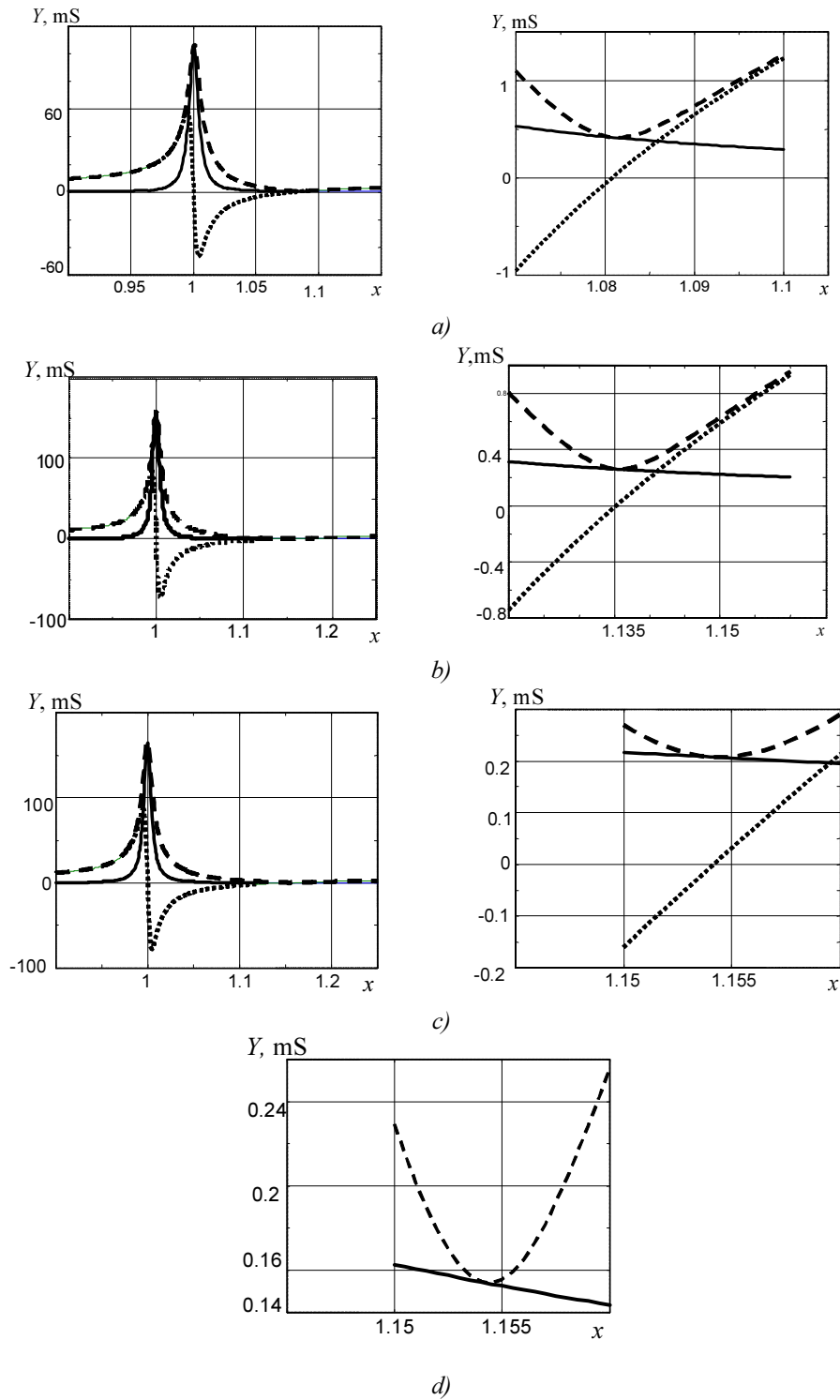


**Figure 3.** Example of admittance changing versus dimensionless frequency during iterative procedure for cylindrical shell of  $18.5 \times 15.7 \times 22$  mm size

**Рисунок 3.** Приклад зміни адмітенсу відносно безрозмірної частоти під час ітераційної процедури для циліндричної оболонки розміром  $18,5 \times 15,7 \times 22$  мм

The For the case  $k_p^2 = 0.3$  (second step, fig.3b) the results  $x_m = 1.0$ ,  $Y_m = 106$  mS,  $x_n = 1.1357$ ,  $Y_n = 0.26$  mS;  $x_n/x_m = 1.1357$  are in low agreement with the experiment data. For case of  $k_p^2 = 0.33$  (third step fig.3c) the results  $x_m = 1.0$ ,  $Y_m = 170$  mS,  $x_n = 1.154$ ,

$Y_n = 0.21 \text{ mS}$ ,  $x_n/x_m = 1.154$  are in agreement with the experimental data. Decreasing of piezoelectric loss tangent to a level  $d_{31m} = 0.0067$  (forth step, fig.3d) can decrease the admittance minimum to value  $Y_n = 0.153 \text{ mS}$ .

The iterative results  $x_m = 1.0$ ,  $Y_m = 170 \text{ mS}$ ,  $k_p^2 = 0.33$ ,  $s_{11m} = 0.0095$ ,  $\varepsilon_{33m} = 0.0104$ ,  $d_{31m} = 0.0067$ ,  $x_n = 1.154$ ,  $Y_n = 0.153 \text{ mS}$ ;  $x_n/x_m = 1.154$  are in very good agreement with experimental data:  $Y_m = 170 \text{ mS}$ ,  $Y_n = 0.14 \text{ mS}$ ,  $f_m = 77.789 \text{ kHz}$ ,  $f_n = 90.039 \text{ kHz}$ ,  $f_n/f_m = 1.1574$ . The deviation for  $Y_m$  is 0%, for  $Y_n$  is 9.3% and for  $f_n/f_m$  is 0.26%.

Thus, for mentioned higher cylindrical shell the next refined data were obtained:  $k_p^2 = 0.33$ ,  $d_{31m} = 0.0067$ ,  $s_{11m} = 0.0095$ .

**Influence of loading regime on admittance and power in frequency range.** Fig.4 demonstrates the admittance's AFCh (left column) and impedance's AFCh (right column) of high ring for regimes «as is» (fig.4a) and after transformation data into regimes of the constant sample current (fig.4b), the constant sample voltage (fig.4c) or the constant sample power (fig.4d) with using formulae (6).

The graphs are plotted for frequency range 50–100 kHz. All four rows on fig.4 are identical, i.e. the admittance and the impedance are independent from loading regime under conditions of small signals.

Fig.5 demonstrates the amplitude-frequency characteristics of instantaneous sample power of high ring for regimes «as is» (fig.5a), the constant sample current (fig.5b), the constant sample voltage (fig.5c) and the constant input voltage (fig.5d). All graphs are very sensitive to loading conditions. In regimes «as is» (fig.5a) and the constant input voltage (fig.5d) the amplitude-frequency characteristics are similar and differ with levels only. The constant sample current (fig.5b) and the constant sample voltage (fig.5c) regimes are characterized with various location of instantaneous power maxima/minima. The power maxima for the case of constant sample current are observed at anti-resonance frequencies and coincide with the power minima for the case of constant sample voltage and vice versa.

The power maxima for constant sample voltage case are observed at resonance frequencies. Such power's behaviour for the constant sample current and the constant sample voltage conditions explains experimental results of Ref [2], where strong admittance's nonlinearity was established.

In the same way it was plotted the angle, current and voltage amplitude-frequency characteristics. The amplitude-frequency characteristics of angles are identical for different loading regimes. Their view is shown on fig.6, where we have used the same notation as in fig.2c. The angle  $\alpha$  (dotted line) is created by  $U_R$  and  $U_{pe}$  sides. The angle  $\beta$  (dashed curve) is created by sides  $U_m$  and  $U_R$ . At last, the angle  $\gamma$  (solid line) is created by sides  $U_m$  and  $U_{pe}$ . Although values  $U_m$ ,  $U_{pe}$  and  $U_R$  are different for different loading regimes their ratios after linear transformation are saved. This is the reason of independence of the admittance, impedance or angles upon loading conditions.

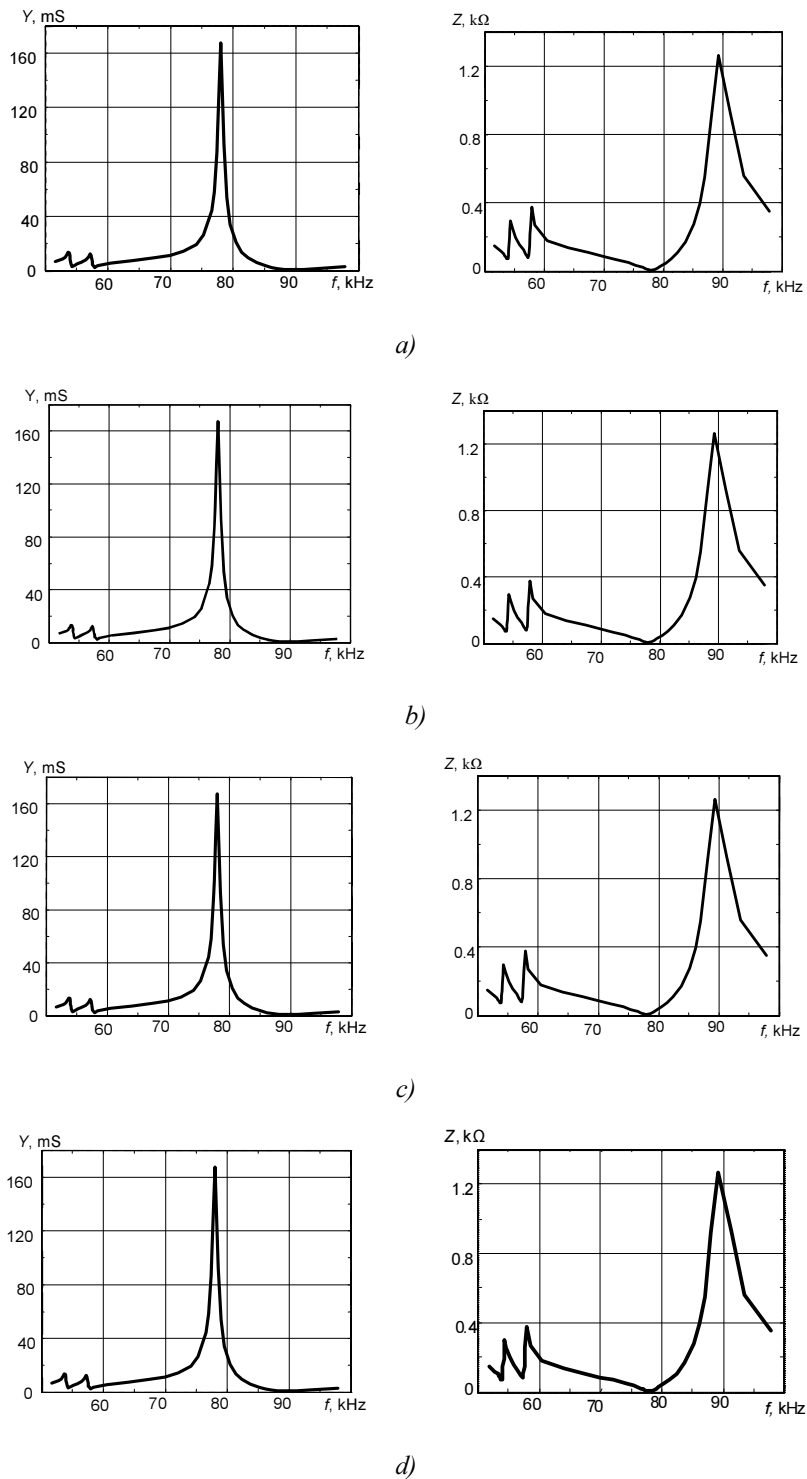


**Figure 4.** Amplitude-frequency characteristics of the admittance (left) and the impedance (right) of high ring for regimes: a) «as is», b) the constant sample current, c) the constant sample voltage, d) the constant input voltage

**Рисунок 4.** Амплітудно-частотні характеристики адмітенсу (зліва) та імпедансу (справа) для високого кільця відповідно для режимів: а) «як є», б) постійного струму зразка, в) постійної напруги зразка, г) постійної вхідної напруги

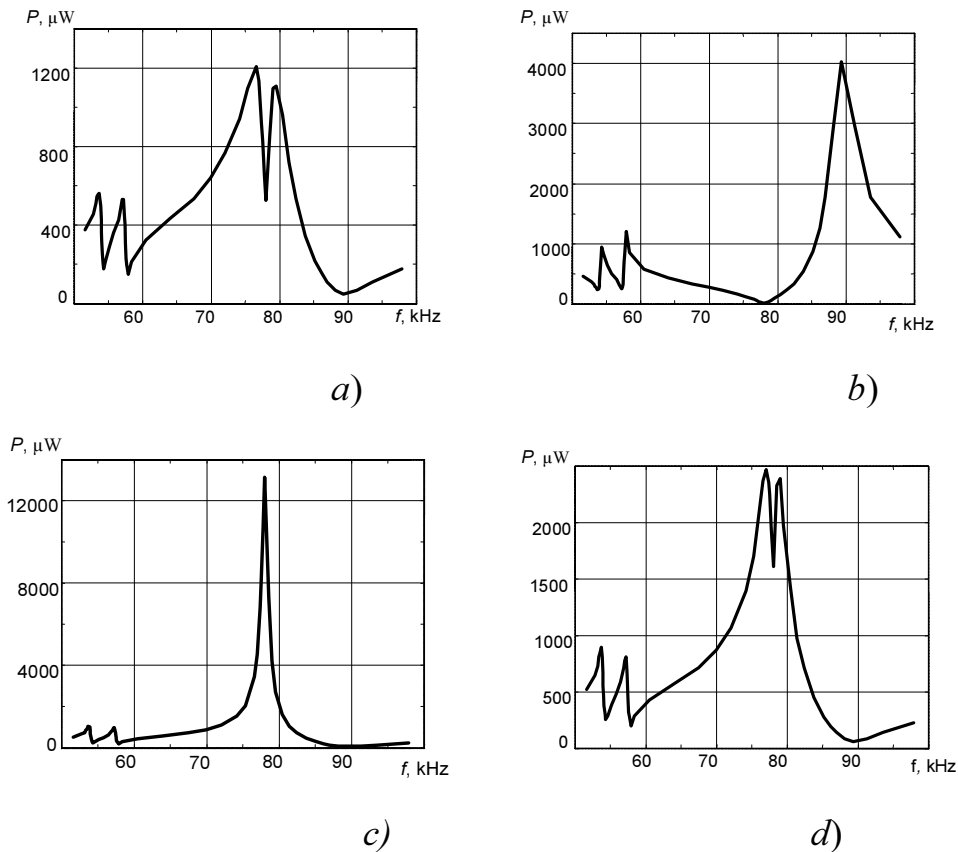


**Figure 5.** Amplitude-frequency characteristics of the instantaneous sample power of high ring for regimes: a) «as is», b) the constant sample current, c) the constant sample voltage and d) the constant input voltage

**Рисунок 5.** Амплітудно-частотні характеристики миттєвої потужності зразка для високого кільця для режимів: а) «як є», б) постійного струму зразка, с) постійної напруги зразка і д) постійної вхідної напруги

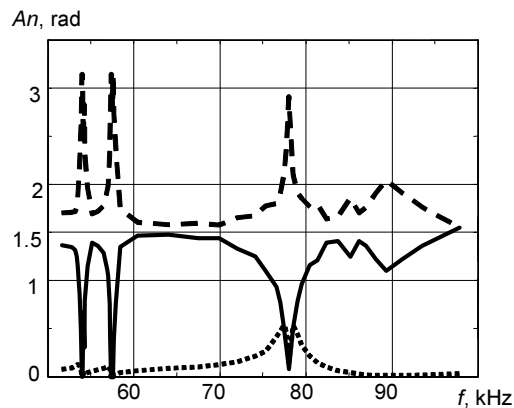


**Figure 6.** Amplitude-frequency characteristics of the angles in the frequency 50–100 kHz range

**Рисунок 6.** Амплітудно-частотні характеристики для кутів у частотному діапазоні 50–100 кГц

**The stress state of cylindrical shells and vibration modes.** Verification of the vibration modes was made with using the method of piezotransformer transducer (sensor) [5,12]. This method enables to determine the distribution of internal stresses for piezoceramic elements from measurements of the surface distribution of charges. For this purpose a number of small electrode-transducers have been divided in an exterior electrode coating of the cylindrical surface. Its potentials and charges are proportional to the sum of

principal stresses [5,6]. The cylindrical rings with radial polarization have longitudinal and azimuth stresses.

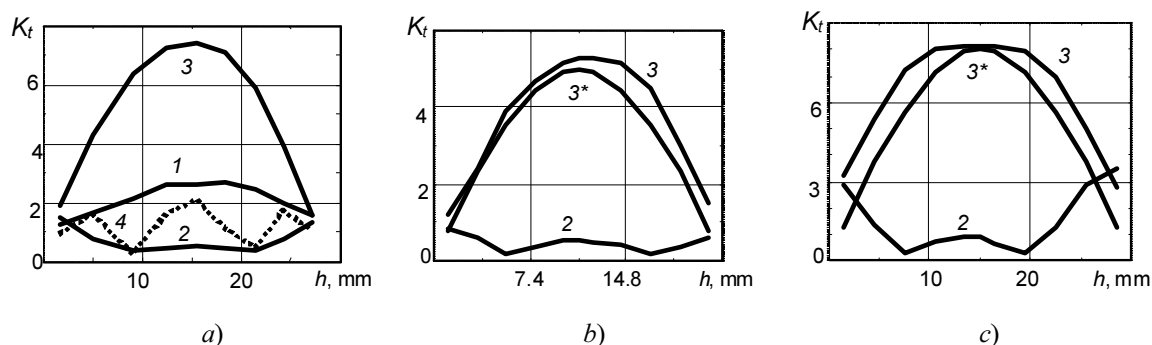


**Figure 7.** Distribution of the transfer ratio  $K_t = V_t/V_0$  versus ring's height  $h$  for the first modes of:

a) short, b) middle and c) high rings

**Рисунок 7.** Розподіл коефіцієнта трансформації  $K_t = V_t/V_0$  відносно висоти  $h$  для перших мод: а) коротких, б) середніх та в) високих кілець

The transfer ratios  $K_t = V_t/V_0$  ( $V_0$  is input potential,  $V_t$  is potential of piezotransformer transducer) are shown in fig.7 for the first modes of short, middle and high rings for frequency 20–200 kHz range. The labels 1–4 denote the number of modes.

The short ring of  $38 \times 34 \times 30$  mm (height/(middle diameter) ratio is 0.882) demonstrates four resonances 25.9, 27.059, 55.789 and 162.913 kHz (fig.7a). At the first resonance interior stresses reach maximum levels in center and they are slowly decreased through. This mode is known as «out of phase» [15], because widening along height surrounds with narrowing in azimuth direction. The dynamic stresses on the second mode are small everywhere except of the ends, where they are sharply increased. This particular mode may be identified as an edge resonance. Being weak for the chosen experimental conditions, this mode is characterized by sharp increase in the amplitude of displacements near the corners and sharp increase in the amplitude of stresses near their ends. The third mode is known as «in phase» [15], because widening along height surrounds with widening in azimuth direction. The fourth mode may be identified as an overtone of the longitudinal vibrations.

The middle ring of  $18.2 \times 15.8 \times 22.2$  mm (height/(middle diameter) ratio is 1.405) has resonances 53.68, 56.965 and 77.868 kHz (fig.7b). The high ring of  $22 \times 18 \times 30$  mm (height/(middle diameter) ratio is 1.66) has resonances 75.281, 76.493 and 93.579 kHz (fig.7c). The label 3\* corresponds to the graph of function  $y = k \cos(x\pi/h)$ , where  $x$  is the running coordinate,  $h$  is sample height, and  $k$  is a matching factor.

The graphs show the greater the ratio of height to middle diameter of the sample the stronger level of edge mode and the larger the distribution of main stress differs from the cosine function.

**Conclusions.** As a result of the experimental study of the forced vibration problem for piezoceramic cylindrical shell rings with radial polarization the following facts can be established.

It is shown that the admittance, impedance and phase angles are independent of the electrical excitation conditions. Sample power, sample voltage and sample current are very sensitive to loading conditions. The instantaneous power reaches the maximum value at resonances for constant sample voltage and at anti-resonances for constant sample current.

This fact explains why the constant voltage regime is surrounded by great nonlinearity but in the constant current regime such phenomena is absent.

The stress state of rings was investigated and the verification of vibration modes was carried out using the piezotransformer-transducer method. It was established that the greater the ratio of height to the middle diameter of the ring, the higher the level of edge mode and the stronger the distribution of main stresses is different from the cosine function. In a very short rings edge mode is not registered.

The proposed technique of research is relatively simple and can be used for engineering design.

**Висновки.** У результаті експериментального дослідження задачі про вимушені коливання п'єзокерамічних циліндричних оболонок у формі кілець з радіальною поляризацією були встановлені наступні факти.

Адмітанс, імпеданс і фазові кути не залежать від умов електричного збудження. Потужність, спад напруги та струм зразка дуже чутливі до умов навантаження. Миттєва потужність досягає максимального значення на резонансах для режиму заданої напруги та на антирезонансах у режимі заданого струму. Цей факт пояснює, чому режим заданої сталої напруги супроводжується значною нелінійністю, а в режимі заданого сталого струму такої нелінійності немає.

Також досліджено напружений стан кілець та верифіковані моди коливань за допомогою методу п'єзотрансформаторного датчика. Чим більше відношення висоти до середнього діаметра кільця, тим вищий рівень крайової моди і тим сильніше розподіл головних напружень відрізняється від косинусоїди. В дуже коротких кільцях крайова мода не реєструється.

Запропонована методика дослідження є достатньо простою і може бути використана при інженерному проектуванні.

## References

1. Uchino, K. Loss mechanisms in piezoelectrics: how to measure different losses separately [Text] / K. Uchino, S. Hirose // IEEE Trans. Ultrason. Ferroelectr. Freq. Control. – 2001. – 48, No. 1. – P. 307–321.
2. Ural, S. O. Development of a high power piezoelectric characterization system and its application for resonance/antiresonance mode characterization [Text] / S. O. Ural, S. Tunodimir, Yu. Zhuang, K. Uchino // Jpn. J. Appl. Phys. – 2009. – 48, No. 5R. – 056509.
3. Uchino, K. Loss mechanisms and high power piezoelectrics [Text] / K. Uchino, J. H. Zheng, Y. H. Chen et al. // J. Mat. Sci. – 2006. – 41. – P. 217–228.
4. Shul'ga, N. A. The vibrations of piezoelectric bodies [Text] / N. A. Shul'ga, A. M. Bolkisev. – Kiev: Naukova Dumka. – 1990. – 228 p.
5. Shul'ga, M. O. Resonance electromechanical vibrations of piezoelectric plates [Text] / M. O. Shul'ga, V. L. Karlash. – Kyiv: Naukova Dumka, 2008. – 270 p.
6. Karlash, V. L. Resonant electromechanical vibrations of piezoelectric plates [Text] / V. L. Karlash // Int. Appl. Mech. – 2005. – 41, No. 7. – P. 709–747.
7. Karlash, V. L. Longitudinal and lateral vibrations of a plate piezoceramic transformer [Text] / V. L. Karlash // Ukr. J. Phys. – 2006. – 51, No. 10. – P. 985–991.
8. Glozman, I. A. Piezoceramics [Text] / I. A. Glozman. – Moscow: Energiya, 1972. – 288 p.
9. Jaffe, B. Piezoelectric ceramics [Text] / B. Jaffe, W. R. Cook, H. Jaffe. – Academic Press: London, 1971. – 142 p.
10. Karlash, V. L. Energy losses in piezoceramic resonators and its influence on vibrations' characteristics [Text] / V. L. Karlash // Electronics and communication. – 2013. – 19, No. 2(79). – P. 82–94.
11. Karlash, V. L. Methods of determination of coupling factors and energy losses at piezoceramics resonator's vibrations [Text] / V. L. Karlash // Acoustic bulletin. – 2012. – 15, No. 4. – P. 24–38.
12. Shul'ga, M. O. Amplitude-phase characteristics of radial vibrations of thin piezoceramics disk near resonances [Text] / M. O. Shul'ga, V. L. Karlash // Reports of the National Academy of Sciences of Ukraine. – 2013, No. 9. – P. 80–86.
13. Shul'ga, M. O. Measurement of piezoceramic elements admittance in Mason's four-pole and its variants [Text] / M. O. Shul'ga, V. L. Karlash // Proc. IY Int. Sci. -tech. Conf. «Sensors, devices and systems» – 2008. – Cherkasy. – Gurzuf, 2008. – P. 54–56.

14. Karlash, V. L. Particularities of amplitude-frequency characteristics of admittance of thin piezoceramic half-disk [Text] / V. L. Karlash // Int. Appl. Mech. – 2009. – 45, No. 10. – P. 1120–1126.

15. Drumheller, D. S. Dynamic shell theory for ferroelectrics ceramics [Text] / D. S. Drumheller, A. Kalnins // J. Acoust. Soc. Am. – 1970. – 47. – P. 1343–1353.

*Отримано 28.04.2015*